Modeling the ring current magnetic field during storms

N. Y. Ganushkina,[1,2] T. I. Pulkkinen,[1] M. V. Kubyshkina,[3] H. J. Singer,[4] and C. T. Russell[5]

Received 28 February 2001; revised 26 June 2001; accepted 27 June 2001; published 2 July 2002.

[1] We present a new model for the inner magnetosphere ring current to get a realistic representation of the magnetic field during storm times. We use a bean-shaped current system, which has cross section that is close to the observed distribution of trapped particles in the inner magnetosphere. The model is symmetric both longitudinally and in the north-south direction, and the current density in the radial direction varies as a Gaussian. The latitudinal distribution of the current density is specified by an "anisotropy index," which is zero for a particle distribution that is isotropic along field lines. Increasing the anisotropy index gives a particle distribution concentrated closer to the equator. We use this method to model the magnetic field evolution during two geomagnetic storms: one on May 2, 1998, when *Dst* reached −80 nT, and the other on May 15, 1997, when it reached −120 nT. The ring current in the Tsyganenko (T89) magnetic field was replaced by our new ring current representation, and the model free parameters are specified using observations from GOES and Polar satellites and *Dst* measurements for each time step separately. We discuss the field configuration changes during the storm, and we evaluate the capability of our modeling technique to represent the large-scale magnetospheric configuration during storm periods. *INDEX TERMS:* 2778 Magnetospheric Physics: Ring current; 2788 Magnetospheric Physics: Storms and substorms; 2740 Magnetospheric Physics: Magnetospheric configuration and dynamics; 2708 Magnetospheric Physics: Current systems; *KEYWORDS:* magnetospheric physics, ring current, storms and substorms, magnetospheric configuration, current systems

1. Introduction

[2] The first ring current magnetic field models implied an a priori predetermined background magnetic field model as well as a given distribution of the energy density of trapped particles in the equatorial plane and their pitch angle distribution function (see review by *Tsyganenko* [1990, and references therein]). The electric current density was calculated based on the guiding center approximation [*Parker*, 1957]. The problem of calculation of the magnetic effect of a distribution of particles trapped in the magnetosphere is not trivial to solve, because the particles move in a magnetic field, a portion of which is due to their motion itself. *Akasofu et al.* [1961] investigated this by successive approximations to the true field, in which the portion of the total magnetic field due to the ring current is determined to successively higher orders until a self-consistent solution has been obtained. *Hoffman and Bracken* [1965, 1967] developed a model to calculate third-order ring current magnetic field for various enhancements in the particle distribution. *Berko et al.* [1975], using the energy density profiles and the pitch angle distributions observed by Explorer 45 during the large magnetic storm on June 17, 1972, calculated the magnetic effects of the proton ring current in a self-consistent manner [*Hoffman and Bracken*, 1967]. These results were obtained using rather sparse particle data sets.

[3] *Mead and Fairfield* [1975] developed the first empirical magnetospheric magnetic field model. They described the contribution from all external sources by a single set of analytical expressions containing quadratic polynomials of solar magnetic coordinates and a linear dependence on the geodipole tilt angle. The model free parameters were calculated by a least squares fitting to the experimental data from the IMP spacecraft measurements sorted by the *Kp* index values. Image dipole models [e.g., *Antonova and Shabansky*, 1968] or the quantitative model by [*Olson and Pfitzer*, 1974] also belong to that category. None of those models contained a clear representation of the ring current magnetic field.

[4] The first empirical model with an explicit ring current based on magnetic measurements was developed by *Tsyganenko and Usmanov* [1982] (TU82 model) and *Tsyganenko* [1987] (T87 model). They used an axially symmetric ring current model represented in cylindrical

[1]Geophysical Research, Finnish Meteorological Institute, Helsinki, Finland.
[2]On leave from Skobeltsyn Institute of Nuclear Physics, Moscow State University, Moscow, Russia.
[3]Institute of Physics, University of St.-Petersburg, St.-Petersburg, Russia.
[4]NOAA, Space Environment Center, Boulder, Colorado, USA.
[5]Institute of Geophysics and Planetary Physics, University of California, Los Angeles, California, USA.

0148-0227/02/2001JA900101$09.00

geomagnetic coordinates (ρ, φ, z) by a vector potential A = (0, A_φ, 0), where

$$A_\varphi = C\rho\left(\rho^2 + z^2 + 4\rho_0^2\right)^{-3/2}. \quad (1)$$

The additional term $4\rho_0^2$, which was the only difference from a purely dipolar vector potential, eliminated the singularity at the origin. The magnetic field components were

$$B_\rho = B_0 \frac{12\rho' z'}{\left(\rho'^2 + z'^2 + 4\right)^{5/2}}, \quad (2)$$

$$B_z = 4B_0 \frac{2z'^2 - \rho'6^2 + 8}{\left(\rho'^2 + z'^2 + 4\right)^{5/2}}, \quad (3)$$

where B_0 corresponded to magnetic field depression at the origin, $\rho' = \rho/\rho_0$, and $z' = z/\rho_0$. The proposed analytical ring current representation gave a ring current distribution with a characteristic radius of the order of ρ_0 localized near the equatorial plane, in accordance with *Sugiura* [1972]. It contained only two parameters, ρ_0 and B_0, and combined mathematical simplicity with its capability to model the main observed features.

[5] Calculations of the electric current distribution during storms [see, e.g., *Lui et al.*, 1987] showed significantly more complex structure of the observed ring current compared to the idealized axially symmetric models. The observed ring current is strongly asymmetric, so that the nightside current dominates by a factor of 2 or 3 [*Iijima et al.*, 1990]. During strongly disturbed periods this asymmetry becomes even larger [*Roelof*, 1987]. Another important feature is the dawn-dusk asymmetry [*Langel and Sweeney*, 1971]. Several attempts to study asymmetries based on spacecraft measurements and partial ring current models were made by, for example, *Tsyganenko and Usmanov* [1984], *Crooker and Siscoe* [1981], and *Harel et al.* [1981]. However, the main aim of these studies was derivation of the large-scale magnetic effects of this current system at geocentric distances 3–7 R_E. Because the asymmetry effects are most pronounced during disturbed periods, the existing database for these conditions was rather small.

[6] *Kosik* [1989] proposed a magnetospheric model in which the magnetic field was expressed as a sum of the toroidal and poloidal terms. This representation was discussed earlier by *Stern* [1976], who showed that the simplest polynomial approximation of the Mead-Fairfield model can be obtained as the sum of poloidal and toroidal fields by a proper choice of the scalar functions. This model was able to obtain good agreement of ΔB contours (external field) with experimental ones [*Sugiura and Poros*, 1973] by a proper choice of the coefficients in the scalar functions. In the ring current region, two components of current flow were present, an eastward flow near the Earth and a westward current in the outer region. The relationship between the functional behavior and the resultant current density distribution was rather complex, because the modification of the model functions had no clear interpretation in terms of current geometry.

[7] *Hilmer and Voigt* [1995] presented a tilt-dependent magnetospheric magnetic field model with the fully shielded vacuum dipole configuration of *Voigt* [1981]. The ring current consisted of eastward and westward currents, each of them symmetric with respect to the Earth's dipole axis, and the representation was similar to that in the TU82 model [*Tsyganenko and Usmanov*, 1982].

[8] Experimental data show a continuous merging of the tail current sheet with the ring current on the nightside [*Speiser and Ness*, 1967; *Fairfield et al.*, 1987]. Earlier, *Sugiura* [1972] and *Sugiura and Poros* [1973] proposed a concept of a single westward equatorial current sheet on the nightside, which approaches the Earth to very close distances. This idea was used in a quite different approach for ring current magnetic field modeling by *Tsyganenko* [1989] (T89 model), based on modification of a vector potential induced by an infinitely thin axially symmetric equatorial current disc. In this representation the ring current and the tail current formed a combined sheet-like system in the near-Earth nightside magnetosphere. However, the steep profile of the electric current density in the vicinity of the inner edge of the current sheet was not reproduced properly, and, as in the earlier versions of the models TU82 and T87, the T89 model lacked the eastward ring current in the inner L shells.

[9] This modeling technique was further developed by *Tsyganenko and Peredo* [1994]. The starting point was to specify a desirable profile for the electric current which made it possible to model a variety of asymmetric magnetic field distributions produced by equatorial current discs with various radial profiles of the electric current density. This model was employed in the T96 [*Tsyganenko*, 1995] magnetic field model for the internal ring current term. The ring current thickness was allowed to vary in the day-night direction. A shift of the whole ring current along the X axis and a scaling of its dimension were introduced. The model ring current was assumed to be centered on the dipole equatorial plane, so that it is inclined with respect to the GSM equatorial plane in response to the Earth's dipole tilt. The ring current amplitude was chosen to be a free parameter. The shielded ring current [*Tsyganenko*, 1995] was then included in the model as an independent term, whose parameters were found together with the tail current parameters by least squares fitting to spacecraft data.

[10] The models described above were not specifically developed for storm time representation. *Alexeev et al.* [1996] proposed a nonstationary model of the magnetospheric magnetic field for the description of storm events. Ring current in this model was calculated in terms of the model similar to TU82, and the dipole field was used beyond a fixed distance. The ring current magnetic field intensity at the Earth's equator was one of the model parameters. The geometry of the ring current was not specified, and the geocentric distance to the ring current maximum and that to the ring current outer boundary were fixed.

[11] Magnetic field modeling for storm events using the current sheet representations of the ring current as it is in the Tsyganenko models, during high Kp with strongly enhanced ring current, results in stretched inner magnetosphere field lines at all radial distances. Part of the enhanced fluxes of trapped particles turn out to be on open or very taillike field lines. These empirical models predict too small a volume of the inner magnetosphere closed flux tubes. *Ganushkina et al.* [2002] suggested modeling the ring current with a toroidal current system with a bi-Gaussian distribution of current

density in cross section. This toroidal representation of the ring current, which is more localized in the radial direction and more distributed away from the equatorial plane, gives positive B_z outside the ring current region. Thus magnetic field lines are stretched only inside the ring current region and are more dipole-like outside, leading to an increased volume of closed flux tubes.

[12] In this paper we introduce a bean-shaped current system, which has a cross section that is close to the observed distribution of trapped particles. In this rather simple model the current density is axially symmetric relative to north-south and longitudinal directions. The principle of magnetic field calculation from this current system is similar to that described by *Ganushkina et al.* [2002], where a toroidal ring current system was suggested. We use this method to model the magnetic field evolution during two geomagnetic storms: one on May 2, 1998, when *Dst* reached −80 nT, and the other on May 15, 1997, when *Dst* dropped to −120 nT. We discuss the ring current system configuration changes during the storm and compare the calculated magnetic field and *Dst* index to observations. We evaluate the capability of our modeling technique to represent the large-scale magnetospheric configuration during storm periods.

2. Ring Current Representation: Model Description

[13] The principles of the present modeling of the ring current system are similar to those in the toroidal model of *Ganushkina et al.* [2002]. Here, instead of using the toroidal representation with a circular cross section, we propose a current system with a "bean-shaped" cross section formed by magnetic field lines which is close to the observed distribution of the trapped particles. We model the ring current as a current system defined on the grid (R, lat, lon) in spherical coordinates, where R is in the range of 2–7 R_E, lat = (−45°, 45°), and lon = (0°, 360°) with the number of grid points of 60 × 50 × 40, respectively. These grid points set a region where the model ring current flows.

[14] In this model we do not introduce a longitudinal dependence of the current density, and the current density is axially symmetric relative to the Z axis in GSM coordinates. In the equatorial plane $Z = 0$ the current density distribution is given by

$$J(R_{eq}) = J_0 \exp\left[-\frac{(R_{eq} - R_0)^2}{2\sigma^2_{R_{eq}}}\right]. \quad (4)$$

This is a normal, or Gaussian, distribution, where $R^2_{eq} = X^2 + Y^2$, J_0 is the maximum current density reached at $R_{eq} = R_0$, and $\sigma_{R_{eq}}$ is the half-width of the current density distribution.

[15] The pitch angle distribution of particles at the equator has been approximated by [see, e.g., *Garcia and Spjeldvik*, 1985]

$$j(\alpha) = j_0 \sin^A \alpha, \quad (5)$$

where $j(\alpha)$ is the directional particle flux, α is the particle pitch angle, j_0 is the maximum particle flux, and A is the anisotropy index. According to conservation of the first adiabatic invariant and the Liouville theorem, the pitch angle distribution at any point on the field line can be found if the pitch angle distribution is known at the equator [*Roederer*, 1970] and the omnidirectional flux, I, on the field line is given by

$$I = I_0 (B/B_0)^{-A/2}, \quad (6)$$

where I_0 is the equatorial flux, B is the magnetic field at a given point, and B_0 is the magnetic field at the equator. Thus isotropic distribution at the equatorial point leads to the isotropic distribution along magnetic field lines.

[16] The current density and the flux density are determined by the particle density. For the current density distribution outside the equatorial plane we assume functional dependence similar to that for the omnidirectional flux given by (6). We assume that the particle density changes along magnetic field lines and that the magnetic

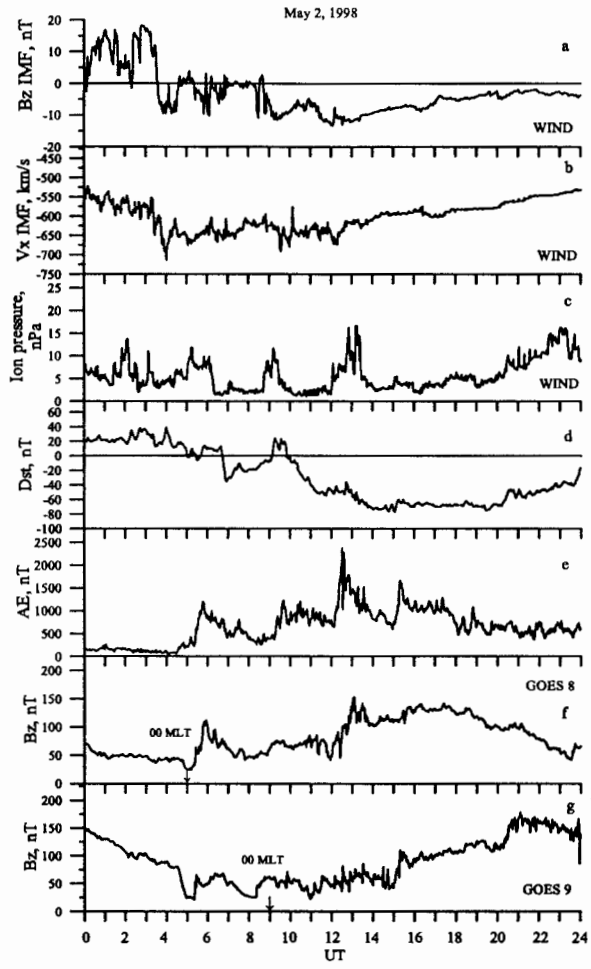

Figure 1. Observational data on May 2, 1998, for the interplanetary magnetic field (a) solar wind velocity V_x (b) and pressure P_{sw} (c) measured by Wind and the *Dst* (d) and *AE* (e) indices, and the B_z component observed by GOES 8 (f) and 9 (g).

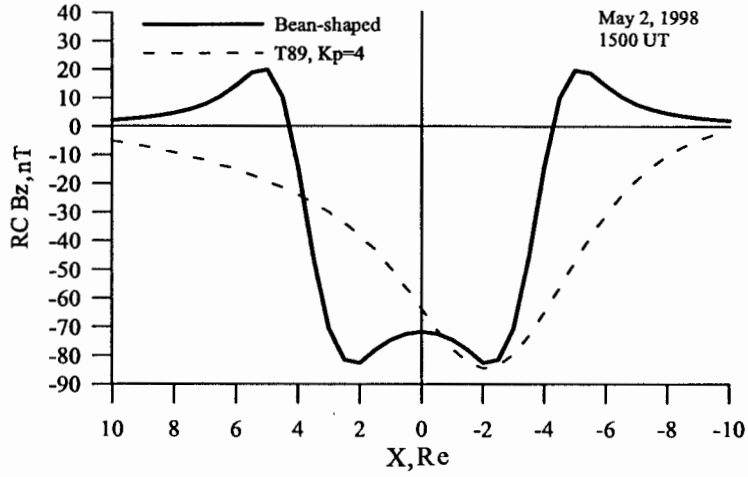

Figure 2. Radial profile of the B_z component of the magnetic field given by the bean-shaped ring current (solid line) and by the T89 ring current for $Kp = 4$ (dashed line). Calculations were made for the May 2, 1998, storm maximum at 1500 UT.

field is dipolar. It is necessary to note here that the described method of ring current magnetic field modeling is not self-consistent. To determine the current density at a given point outside the equatorial plane, we first trace the corresponding magnetic field line to the equatorial plane and find the equatorial distance and the magnetic field at this corresponding equatorial point. Then we can find the ratio(B/B_0). In the dipole field this ratio is connected to the latitude λ of

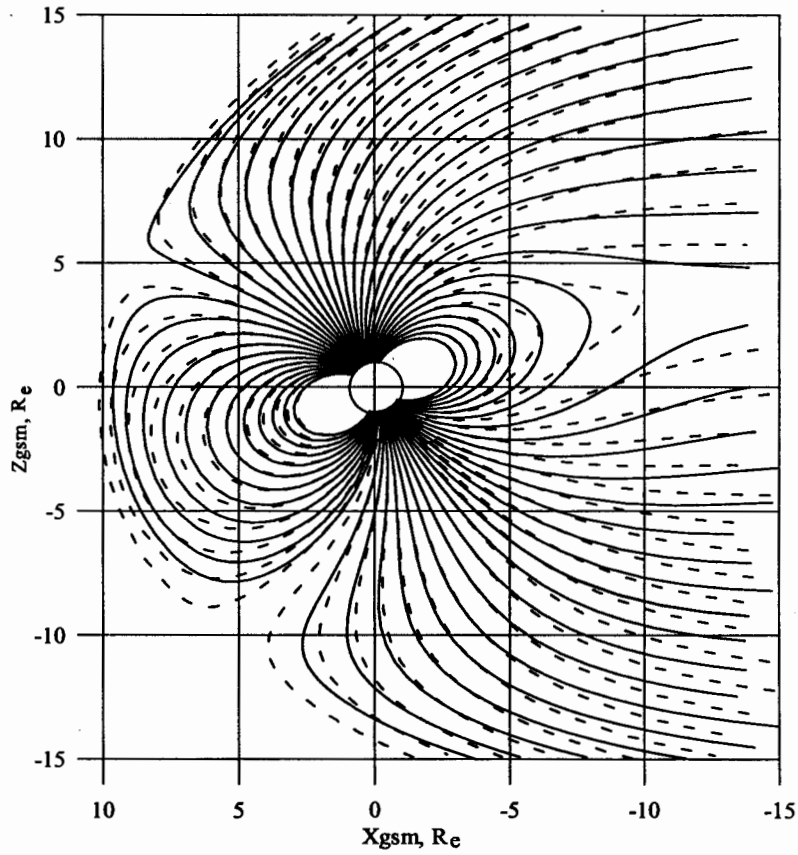

Figure 3. Magnetic field line configuration given by Tsyganenko (T89) $Kp = 4$ model (dashed lines) and modeled with bean-shaped ring current and variations of other current systems (solid lines) for the same May 2, 1998, storm maximum at 1500 UT.

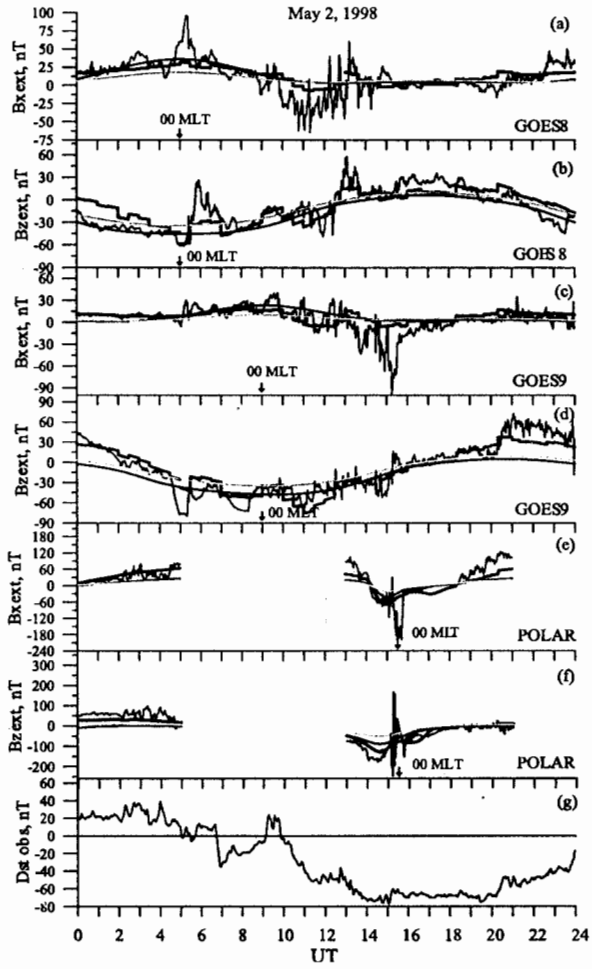

Figure 4. The B_x and B_z components of measured external magnetic field (solid black lines), modeled with bean-shaped ring current and variations of other current systems as described above (red lines) and modeled using Tsyganenko (T89) magnetic field model for Kp = 2 (green lines) and Kp = 4 (blue lines) for (a, b) GOES 8, (c, d) GOES 9, and (e, f) Polar measurements when data were available during storm event on May 2, 1998, with (g) the *Dst* index variations. See color version of this figure at back of this issue.

the given point $B/B_0 = \frac{\left[4-3\cos^2\lambda\right]^{1/2}}{\cos^6\lambda}$. Thus, if we know the current density distribution in the equatorial plane $J(R_{eq})$ (equation (4)), we find the current density at a point outside the equatorial plane as

$$J(B/B_0) = J(R_{eq})(B/B_0)^{-A/2}. \quad (7)$$

Latitudinal dependence of the current density is given by the "anisotropy index" $A/2$ in (7). If A is equal to 0, particle distribution is isotropic along the field lines (the same as at the corresponding point at the equator). Increasing A leads to particle distributions concentrated closer to the equator.

[17] The magnetic field from this current system is calculated from the Biot-Savart law. In order to attribute each grid element of the ring current system with the value of the current, we integrate the current density J over the vicinity dS of the element. We then calculate the contributions from all current elements at a given point. If in the vicinity of the given point there are elements within distances smaller than the distance between elements, we exclude their contribution from the magnetic field calculation at this point. This helps to avoid irregularities in the magnetic field which arise when approaching singular points where the actual current flows.

[18] For this ring current representation the following parameters are, in principle, variable: mean radius of the maximum current density, R_0, the maximum current density, J_0, the width of the Gaussian distribution, σ_R, and the "anisotropy index," A.

3. Magnetic Field Modeling for Storm Time Events

[19] To test our model we selected two storm events, which occurred on May 2, 1998, and May 15, 1997. We modeled 24 hours around the peak activity. We used the Tsyganenko T89 magnetospheric magnetic field model for Kp = 4 as a baseline model, and we replaced the original representation of the ring current with the "bean"-shaped ring current. This substitution was easy enough to do as the T89 model consists of separate terms for external current systems. The more recent model of Tsyganenko T96 parameterized by solar wind dynamic pressure, B_y and B_z components of interplanetary magnetic field, and *Dst* index contains more complex analytics and shielding terms, and it is much more difficult to introduce another current system and change the existing current systems inside the model. To reduce the number of free parameters, for the ring current representation we set $R_0 = 3.8\ R_E$, $\sigma_R = 0.8$, and $A/2 = 1$. We varied J_0 in the range between 1.2 and 15 nA m^{-2}. In addition to storm time changes in the "bean"-shaped ring current, we introduced changes in other current systems such as tail current and magnetopause currents in a manner similar to that used by *Pulkkinen et al.* [1992]. During our modeling we varied the intensity of the tail current and its closure along the nightside magnetopause in response to the changes associated with substorm activity. The magnetopause moves inward during increased solar wind dynamic pressure. To adjust this, we varied the intensity of the Chapman-Ferraro currents at the magnetopause. Tail current amplification factor was (1 + ATS), where ATS varied between −0.40 and 2, and magnetopause current amplification factor (1 + AMP) had AMP in the range between −0.2 and 1. ATS and AMP values indicate the change of tail and magnetopause currents from the original values, i.e., those given by Tsyganenko T89 Kp = 4 model. If ATS and AMP are equal to zero, the tail and magnetopause currents are the same as those of Tsyganenko T89 model.

[20] By varying the parameters described above we found the set of parameters that gives the best fit between the model and the in situ field observations by GOES 8, GOES 9, and Polar satellites and the *Dst* measurements (obtained from the World Data Center C2 for Geomagnetism, Kyoto). The procedure was as follows. We started the search procedure from different initial sets of model parameters randomly generated by Monte Carlo method. We

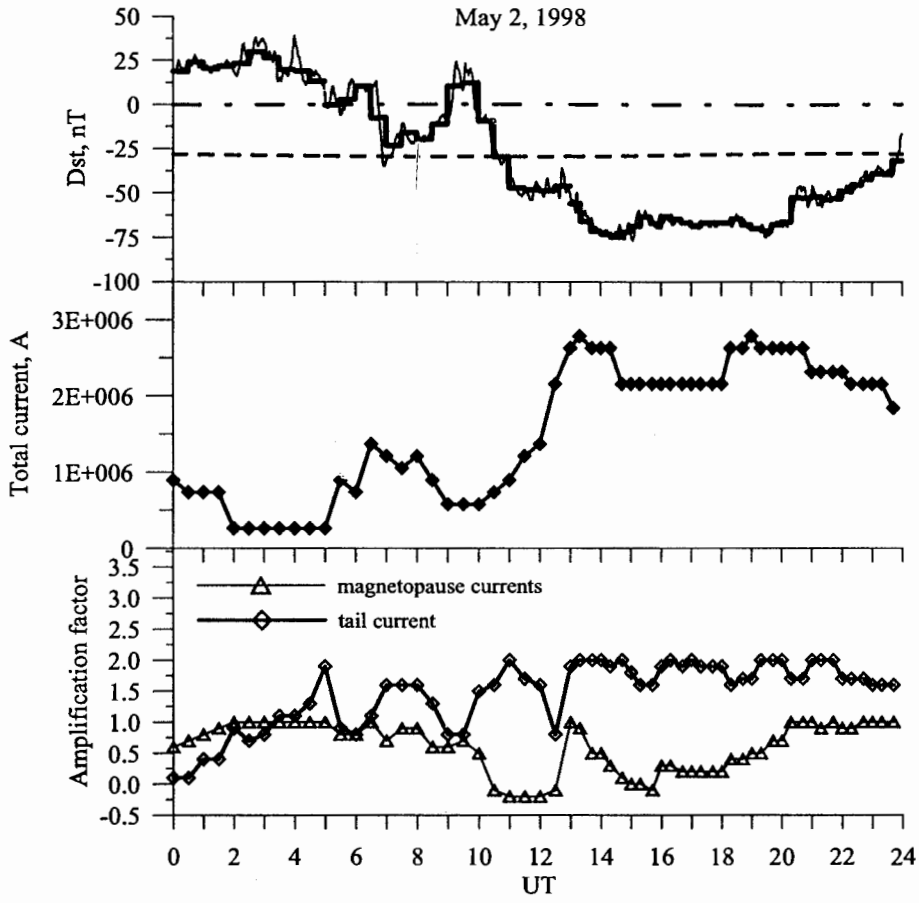

Figure 5. (top) Observed *Dst* index (thin solid line), modeled using bean-shaped ring current with variations of other current systems (thick solid line) and using Tsyganenko (T89) magnetic field model for $Kp = 2$ (dash-dotted line) and $Kp = 4$ (dashed line). (middle) Variations of total current in the bean-shaped ring current system. (bottom) Tail current (line with squares) and magnetopause currents (line with triangles) changes during the modeling on May 2, 1998.

found the set of parameters, which gave the minimum deviation between the modeled and the observed magnetic field values. Then, in this set of fixed parameters one of them varied in the corresponding range in order to find the parameter meaning giving the minimum error between the model and the observations. With that parameter fixed, the next parameter was varied. The procedure was repeated for all parameters. As a result, we had a new set of parameters, different from the initial one. The procedure was repeated once more, but the parameters varied in the vicinity of the previously obtained values with smaller step. In principle, it is possible to repeat the procedure several times for better accuracy, but the computation time then becomes quite long. The danger of getting into local minimum always exists while solving the problems of this kind. In our case we really avoided it combining two methods. Moreover, we controlled the error value on each step of calculations.

3.1. May 2, 1998, Storm Event

3.1.1. Event description

[21] The storm in early May 1998 was initiated from an extended period of solar activity which started on April 29. There were several coronal mass ejections during the period: April 29 (1700 UT), May 1 (2340 UT), May 2 (0530 UT), and May 4 (0200 UT). Here we concentrate on the period May 2, 0000–2400 UT. Figure 1 shows the interplanetary magnetic field B_z component, solar wind velocity V_x, and pressure P_{sw} measured by Wind, the *Dst* and *AE* indices, and the B_z (*GSM*) component observed by GOES 8 and 9. The activity was driven by a magnetic cloud, whose effects were first seen at 0335 UT when IMF B_z turned southward. After that the IMF B_z was close to zero and fluctuated until 0800 UT and then remained southward at about -10 nT for more than eight hours. The solar wind velocity was around 600 km s^{-1}. Solar wind dynamic pressure showed several peaks at 15 nPa. The *Dst* index became negative at 0640 UT, reaching -35 nT, and then increasing to 24 nT at 0915 UT. Then it decreased, reaching -80 nT at 1500 UT, and recovered to the level of about -20 nT by the end of the day. The magnetospheric response was seen as a strong increase in the *AE* index that reached over 2000 nT. Correspondingly, the geostationary magnetic field measurements show sub-

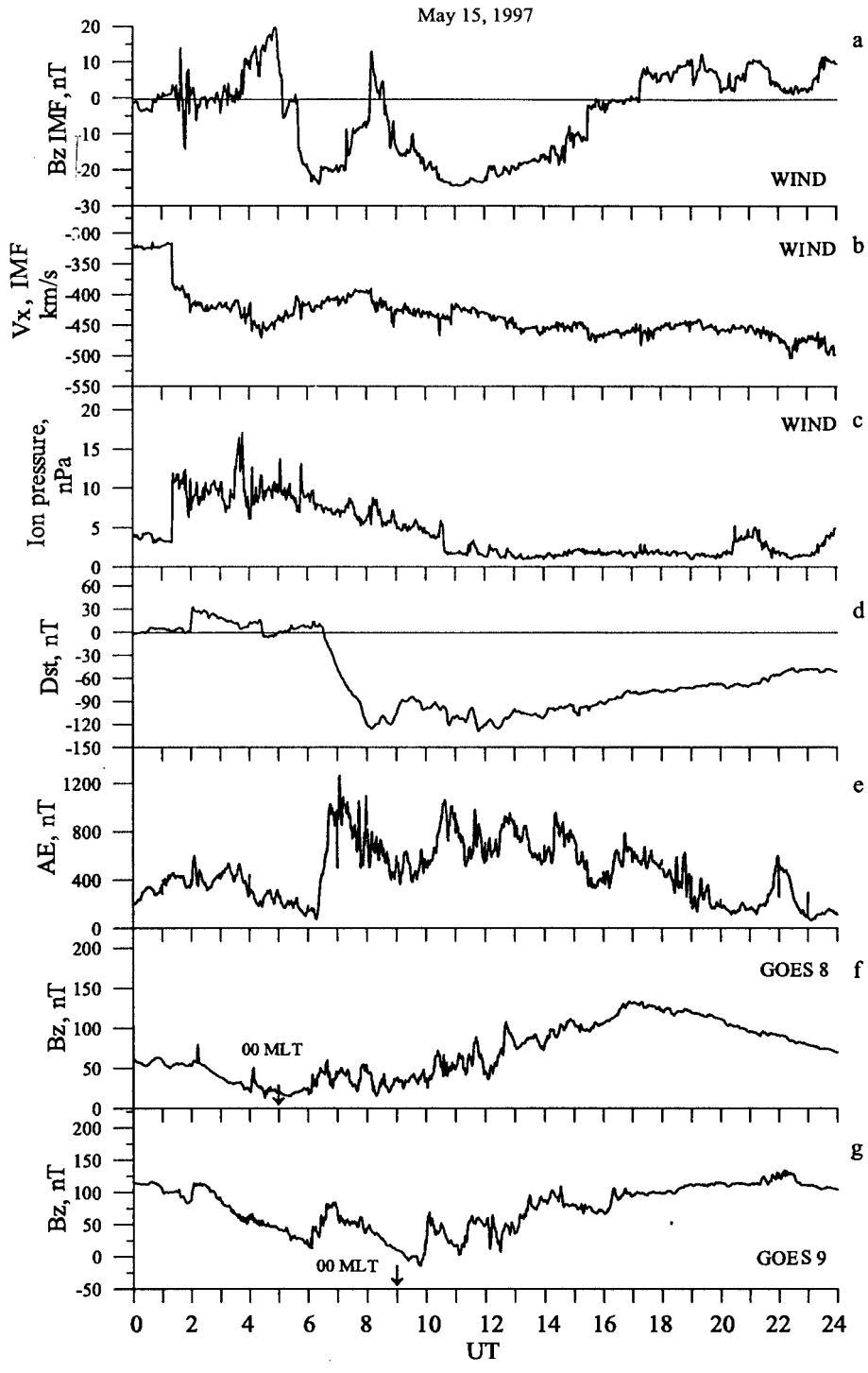

Figure 6. Overview of the storm on May 15, 1997. (a–c) B_z component of the interplanetary magnetic field, velocity V_x, and solar wind dynamic pressure P_{sw} as measured by Wind, respectively. (d, e) *Dst* and *AE* indicies. (f, g) Geosynchronous magnetic field measurements from the GOES 8 and 9 spacecraft.

storm behavior in B_z at the beginning of the day when GOES 8 and 9 were on the nightside.

3.1.2. Model results: Radial profile of B_z component

[22] Figure 2 shows the radial profile of the B_z component of the magnetic field given by the bean-shaped ring current and by the T89 ring current for $Kp = 4$ at the time of the storm maximum on May 2, 1998, at 1500 UT. The following parameters of the bean-shaped ring current were set: half-width of Gaussian distribution $\sigma_R = 0.8$ and maximum current density $J_0 = 13$ nA m^{-2}. The tail current

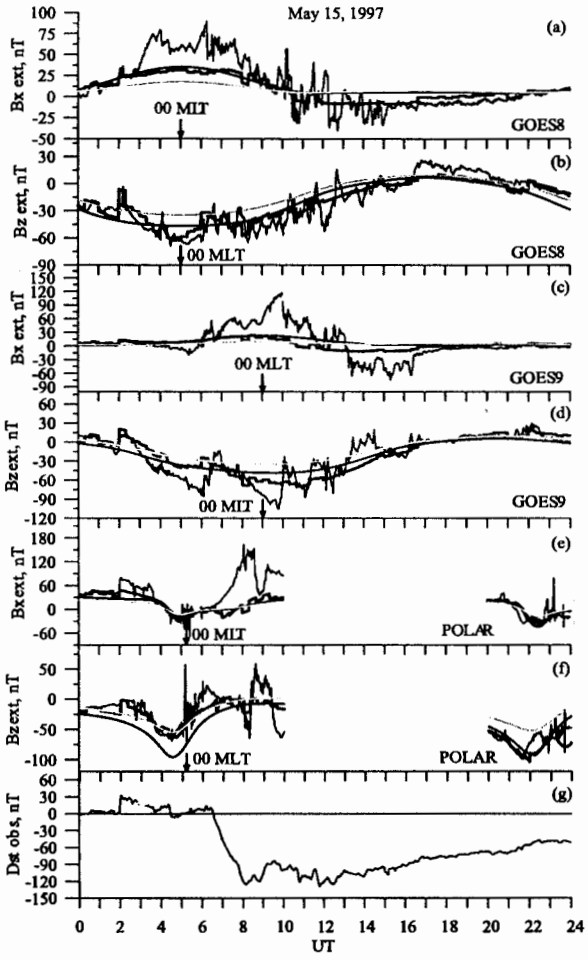

Figure 7. The B_x and B_z components of the measured external magnetic field (solid black lines), modeled with the bean-shaped ring current and variations of other current systems as described above (red lines) and modeled using Tsyganenko (T89) magnetic field model for $Kp = 2$ (green lines) and $Kp = 4$ (blue lines) for (a, b) GOES 8, (c, d) GOES 9, and (e, f) Polar measurements when data were available with (g) the *Dst* index variations during the modeled event on May 15, 1997. See color version of this figure at back of this issue.

was increased by a factor of 2.8 (ATS = 1.8), and the magnetopause currents were the same as those by Tsyganenko T89 $Kp = 4$ model. The Tsyganenko T89 $Kp = 4$ model gives a negative B_z of the ring current everywhere in the inner magnetosphere, which results in field line stretching inside and outside the ring current region. In the T89 model the effects of the day-night asymmetry were incorporated in the ring current model by allowing the current sheet thickness to be a function of X_{SM}, like in the tail sheet model. The B_z minimum is shifted tailward. In the bean-shaped ring current system there is no day-night asymmetry. The bean-shaped ring current produces positive B_z outside the ring current region, which provides more dipole-like field lines there. Figure 3 shows the magnetic field line configuration given by the Tsyganenko T89 $Kp = 4$ model and the bean-shaped ring current and variations of other current systems for the same May 2, 1998, storm maximum at 1500 UT. Magnetic field lines are less stretched for the bean-shaped ring current model both on the nightside and on the dayside. Thus the model reproduces the observed increased volume of trapped particles.

3.1.3. Model results: Magnetic field, *Dst*, and ring current parameters

[23] Figure 4 shows the B_x and B_z components of the measured external magnetic field, for the bean-shaped ring current model and for the Tsyganenko T89 model for $Kp = 2$ and $Kp = 4$ compared to GOES 8 (Figures 4a and 4b), GOES 9 (Figures 4c and 4d), and Polar (Figures 4e and 4f) measurements. Figure 4g shows the *Dst* index variations during the event on May 2, 1998. The bean-shaped ring current model tends to follow the substorm-associated variations in B_x and B_z components, and thus, at many intervals this model represents the observed field better than the Tsyganenko T89 model. At the same time, during most activations the model field underestimates the observed B_x and B_z depressions and enhancements. This is partially owing to the fact that in our modeling we change the ring and tail currents globally, which leads to smaller local variations than if more localized currents were placed close to the spacecraft locations.

[24] The top panel of Figure 5 shows the observed *Dst* index, *Dst* computed from the bean-shaped ring current, and *Dst* computed from the Tsyganenko T89 model for $Kp = 2$ and $Kp = 4$. To get the model *Dst* index the magnetic field was calculated at the Earth's surface at the locations of several stations such as Sun Juan, Tenerife, Tbilisi, Lunping, Kakioka, Honolulu, and Dell Rio. The induced currents on the ground were not taken into account when calculating *Dst*. It was assumed that as the T89 model does not contain the eastward part of the ring current, the induced current contribution to *Dst* can be compensated by the eastward ring current. For the quiet time level we used the magnetic field given by Tsyganenko T89 magnetic field model for $Kp = 2$. The modeled *Dst* index then represents almost exactly the observed *Dst* behavior.

[25] The middle panel in Figure 5 illustrates the variations of total current in the bean-shaped ring current system. At the beginning of the day when *Dst* was positive, the total current was $\sim 3\ 10^5$ A. It increased up to $1.5\ 10^6$ A during the *Dst* decrease at ~0500–0700 UT. At 0915 UT, *Dst* became positive for ~1 hour, and the total current decreased to $6\ 10^5$ A during that period. *Dst* decreased again, and total current increased to $2.5\ 10^6$ A and persisted at that level until the end of the day.

[26] The bottom panel in Figure 5 demonstrates how the tail current and magnetopause currents were changed during the modeling. The line with squares shows the ATS parameter in the tail current amplification factor (1 + ATS). The ATS variations approximately follow *AE* index variations (increased tail current during increased *AE*), illustrating that the tail current changes are associated with substorms. Magnetopause currents were increased by a factor of ~2 (AMP = 1) during the first 10 hours of the day while solar wind pressure showed variations with

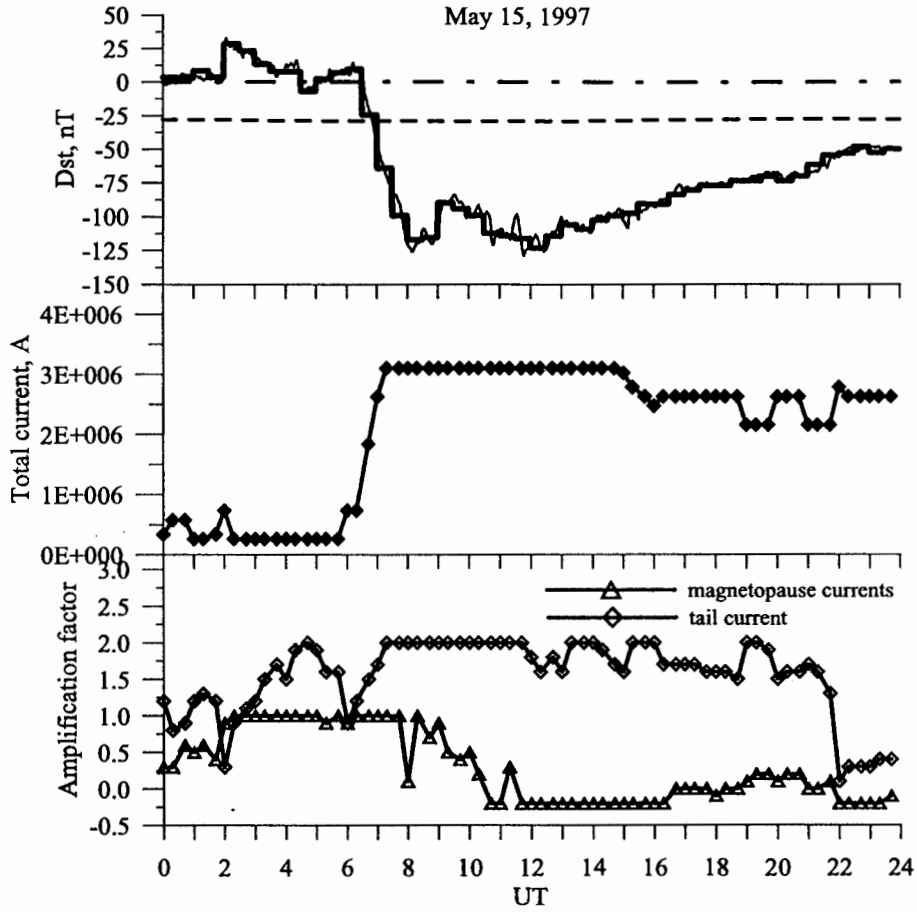

Figure 8. (top) Observed *Dst* index (thin solid line), modeled using "bean-shaped" ring current with variations of other current systems (thick solid line) and using the Tsyganenko T89 magnetic field model for $Kp = 2$ (dash-dotted line) and $Kp = 4$ (dashed line). (middle) Variations of total current in the bean-shaped ring current system. (bottom) Changes in the tail current (line with squares) and magnetopause currents (line with triangles) during the modeling on May 15, 1997.

peaks up to ~10–12 nPa. Then the amplification factor started to decrease, and during the second decrease of *Dst* at 1000–1200 UT, magnetopause currents were slightly smaller than Tsyganenko T89 magnetopause currents for $Kp = 4$. A sharp increase at ~1230 UT corresponds to the maximum solar wind pressure (17 nPa) observed at about that time. The following negative *Dst* period and further recovery were accompanied by decreasing magnetopause currents to the Tsyganenko T89 $Kp = 4$ level and gradual increasing toward the end of the day.

3.2. May 15, 1997, Storm Event

3.2.1. Event description

[27] This geomagnetic storm was driven by a magnetic cloud that followed a coronal mass ejection from the Sun on May 12, 1997. Figure 6 shows an overview of the storm on May 15, 1997. Figures 6a–6c show the B_z component of the interplanetary magnetic field, velocity V_x, and solar wind dynamic pressure P_{sw} as measured by Wind, respectively. The measurements show a very sharp rise in V_x and P_{sw} at 0115 UT, which is identified as a strong shock wave in front of the cloud. The solar wind dynamic pressure increase compressed and greatly distorted the magnetosphere. Following the shock wave arrival, there were very strong, rapid fluctuations in B_z and P_{sw}. After reaching values over 15 nPa, the solar wind dynamic pressure diminished to 2 nPa by 1000 UT. At about the same time, B_z became much smoother and less fluctuating and began a steady rotation from strong southward (−25 nT) to northward (10 nT). As the cloud reached the Earth, the magnetosphere responded with an increased level of activity as recorded by *Dst* and *AE* indices (Figures 6d and 6e). The *Dst* index dropped to below −120 nT by 1200 UT. The *AE* index shows several substorm activations more than 1000 nT in amplitude. Figures 6f and 6g display the geosynchronous magnetic field measurements from the GOES 8 and 9 spacecraft. Particularly notable were the large-amplitude fluctuations nearly 50 nT peak to peak in the field magnitude. They started at 0600 UT and persisted until ~1500 UT. This suggests that large inductive electric fields should be present near geostationary orbit. GOES 9 data show sub-

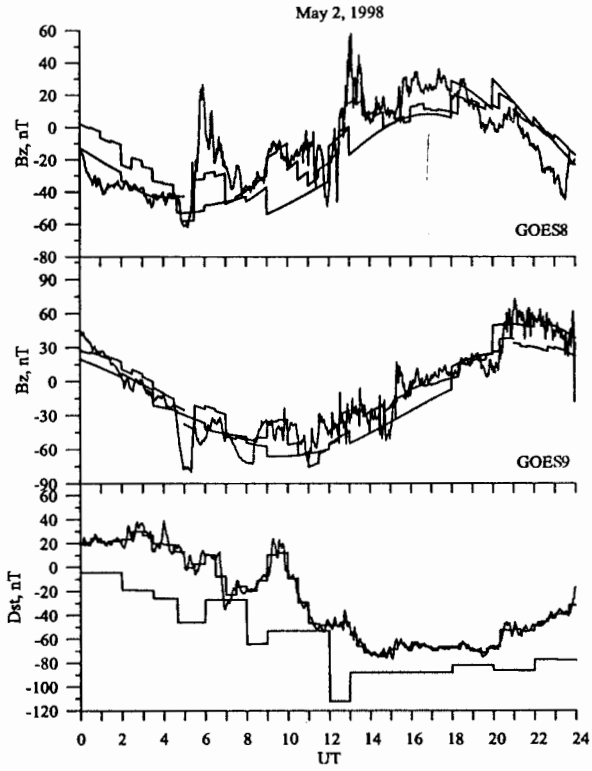

Figure 9. Observed B_z component of magnetic field (black lines), that modeled by using the bean-shaped ring current (red lines), and that calculated using the T96 model (pink lines) for GOES 8 data (top panel) and GOES 9 data (middle panel). The bottom panel shows the corresponding *Dst* index for the storm event on May 2, 1998. See color version of this figure at back of this issue.

storm behavior of B_z during the period the spacecraft was in the nightside magnetosphere.

3.2.2. Model results: Magnetic field, *Dst*, and ring current parameters

[28] Figure 7 shows, in the same format as Figure 4, B_x and B_z components of the measured external magnetic field (solid black lines), for the bean-shaped ring current model (red lines), and for the Tsyganenko T89 model for $Kp = 2$ (green lines) and $Kp = 4$ (blue lines) compared with GOES 8 (Figures 7a and 7b), GOES 9 (Figures 7c and 7d), and Polar (Figures 7e and 7f) measurements. Figure 7g shows the *Dst* index variations during the event on May 15, 1997. Again, the model is in relatively good agreement with the observed magnetic field (although not as good as for the May 2, 1998, storm).

[29] The top panel in Figure 8 shows the observed *Dst* index, the bean-shaped ring current model, and the Tsyganenko T89 model for $Kp = 2$ and $Kp = 4$. Again, the modeled *Dst* index agrees well with the observed one. The middle panel in Figure 8 illustrates the variations of total current in the "bean-shaped" ring current system. During positive or close to zero, *Dst* total current was $\sim 2.5\ 10^5$ A. It increased up to $3\ 10^6$ A during the mainphase of the storm and slightly decreased during the recovery. Compared to the May 2,1998, storm, this event has higher current for lower (more negative) *Dst*.

[30] The bottom panel in Figure 8 presents the changes in the tail current and magnetopause currents. The ATS variations again follow approximately the *AE* index variations (increased tail current during increased *AE*) showing the substorm tail current changes (see, for example, at 0600 UT). During the storm main phase the tail current is increased up to 3 times the T89 model value (ATS = 2). Magnetopause currents were increased by a factor of ~ 2 when the solar wind pressure was increased, and they varied around 10 nPa. Then, with decreasing solar wind pressure to 2 nPa and increasing *Dst*, the magnetopause currents started to decrease at $\sim$0800 UT and were about 0.8 (AMP = -0.2) of the Tsyganenko T89 magnetopause currents for $Kp = 4$. Around 2000 UT a small increase by 1.2 times corresponded to a solar wind pressure increase at that time.

4. Discussion and Conclusions

[31] In this paper we introduced a bean-shaped ring current system, which has a cross section that is close to the observed distribution of trapped particles. The magnetic field from this current system is calculated by using the Biot-Savart law. We modeled magnetic field changes during two storm events on May 2, 1998, and May 15, 1997, replacing the Tsyganenko T89 $Kp = 4$ model representation of ring current with a bean-shaped ring current. For our modeling we had three free parameters: One of them is the parameter defining the ring current density distribution, the intensity of the tail current and its closure along the nightside magnetopause, and the intensity of Chapman-Ferraro currents. During the modeling of storm events we varied only the maximum current density (from which the total current was calculated), tail current, and magnetopause current.

[32] In principle, our model may contain a good number of free parameters which could represent the geometry and distribution of current in the ring current system. However, both the ground magnetic measurements used to determine *Dst* and the GOES spacecraft are mainly outside the ring current. Moreover, GOES spacecraft are situated close to each other. This does not allow us to resolve the spatial characteristics of ring current system. It is difficult to separate effects of moving the current system closer to the Earth from effects of intensification of the total ring current. Thus the possibility to increase the number of variable parameters is limited by observations available. Increasing the number of free parameters also strongly increases the computation time for each time step.

[33] Owing to the same reason, the bean-shaped ring current model does not contain local time asymmetries. In principle, it is possible to include asymmetries in the model, and we are planning to do it. In the T89 model the effects of the day-night asymmetry were incorporated in the ring current model by allowing the current sheet thickness to be a function of X_{SM}, similarly to the tail sheet model. Because our magnetic field calculations are numerical, we could, in principle, set any current distribution in space. We only have to satisfy the current continuity condition. If we would like to take into account current

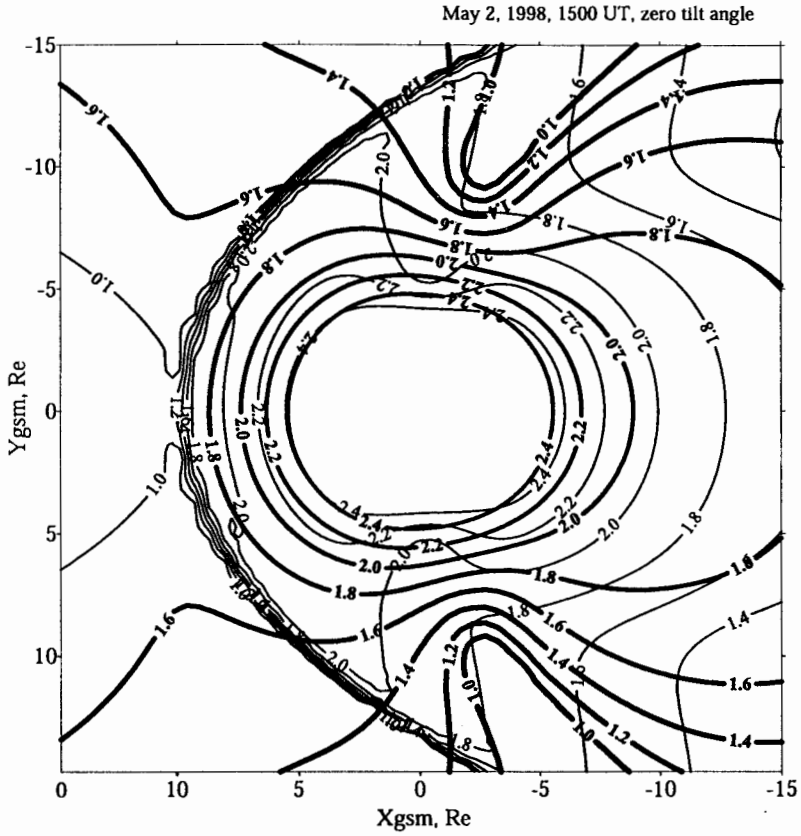

Figure 10. The B = const contours in the equatorial plane calculated using the T96 model (thin lines) and the T89 model for $Kp = 4$ with a bean-shaped ring current with variations of other current systems (thick lines) for the storm maximum at 1500 UT on May 2,1998. The observed solar wind parameters and *Dst* index were used as parameters of the T96 model. Labels on the contours correspond to $log_{10}B$, so that 2.0 corresponds to 100 nT of the magnetic field, 1.8 to 63 nT, etc.

density dependence on local time, we should think about current closure, i.e., to include, for example, field-aligned currents. One possibility for studying the asymmetries in the ring current would be to use magnetograms from several stations around the Earth instead of *Dst* index. The results obtained in the statistical study by *Tsyganenko et al.* [1999] based on data of Polar on the inner magnetic field asymmetries can be very useful for checking and parameterizing our model.

[34] The Tsyganenko T89 $Kp = 4$ model with the ring current replaced by a bean-shaped ring current gives a good *Dst* index and a relatively good magnetic field with the appropriate choice of model parameters by fitting to observations. Model parameters also exhibited typical behavior. The total current in the ring current increased when *Dst* decreased, and it was maximum ($\sim 3 \times 10^6$ A) during the storm maximum. The tail current increases and decreases following the corresponding changes in *AE* index. The tail current was largest during the storm main phase (3 times larger than that in the T89 model). Note that the large enhancements of the tail current relative to the T89 values are partially caused by the fact that the ring current module in the original T89 model was removed from the version we used (replaced with the bean-shaped ring current). As described in section 1, the T89 current discs all extend to the inner and middle magnetotail, and hence removing thering current module also reduces the inner tail currents. The magnetopause current increases correlated with solar wind pressure changes, and during increased solar wind pressure (10–15 nPa) the magnetopause currents were twice as big as those inthe T89 model.

[35] At the same time, during most activations the model field underestimated the observed B_x and B_z depressions and enhancements. In our modeling we changed the ring current globally, not taking into account local changes of the current systems. Furthermore, ring current asymmetries were not present, and there was no partial ring current. Since we used input data from three locations in space and several on ground, the optimal fit represents an average large-scale current system that ignores large intensifications caused by localized disturbances. In this paper we have attempted to obtain an optimal model for thelarge-scale current systems in the entire magnetosphere. If the model would be used to study processes localized in a particular region, observations for that region can be given additional weight, which would then result in a better response to the localized variations.

[36] The Tsyganenko T96 model gives the magnetic field as a function of solar wind and activity parameters.

Figure 9 shows the observed B_z component of the magnetic field, the bean-shaped ring current model, and the T96 model for GOES 8 (top panel) and GOES 9 (middle panel). The bottom panel shows the corresponding *Dst* indices. The day of May 2, 1998, was divided into 12 intervals. Within each interval the parameters for the T96 model were determined on the basis of observations. The calculated *Dst* using the T96 model overestimates considerably the observed *Dst* index. This shows that the model does not represent the magnetic field configuration correctly even if it uses the observed parameters as the input. It produces magnetic field variations that are quite close to observations, but on the whole the bean-shaped ring current gives a better representation of the dynamics.

[37] Magnetic field modeling for storm events using the Tsyganenko magnetospheric magnetic field models with strongly enhanced ring current during high *Kp* results in stretched inner magnetosphere magnetic field lines both on the nightside and on the dayside. Thus, when compared to particle observations, part of the enhanced fluxes of trapped particles turn out to be on open or very taillike field lines. To illustrate this, we plotted in Figure 10 B = const contours in the plane $Z = 0$ in *GSM* coordinates calculated using T96 model and the bean-shaped ring current model with parameters corresponding to the storm maximum at 1500 UT on May 2, 1998. The observed solar wind parameters and *Dst* index were used as input parameters for the T96 model. The tilt angle was set equal to zero, which allows us to look on the particle trajectories in the equatorial plane. Labels on the contours correspond to $log_{10}B$, so that 2.0 corresponds to $B = 100$ nT. Let us consider the drift of particles with 100-keV energy in the equatorial plane. Under gradient drift, protons move westward, electrons move eastward, and they follow the B = const contours. For the T96 model even the $B = 100$ nT countour is not closed, and thus the drifting particles remain trapped in the inner magnetosphere only during their nighttime pass, and they escape from the magnetosphere on the dayside. The bean-shaped ring current produces positive B_z outside the ring current region, which provides more dipole-like field lines there. Magnetic field lines are less stretched for the bean-shaped ring current model both on the nightside and on the dayside. The $B = 100$ nT contour is closed aswell as the next contour with label 1.8 (~63 nT) shown in Figure 10. Particles on these drift trajectories remain trapped, increasing the global ring current.

[38] This model has been developed to study the dynamics of the magnetospheric plasma during storms and substorms by numerical tracing of particle orbits in the inner magnetosphere [*Ganushkina et al.*, 2001]. Particle convection paths are different, for example, for dipole and more realistic magnetic fields. The use of more realistic models might help to keep particles trapped [*Jordanova et al.*, 1998], to take into account the high-energy particle (>~ 100 keV) contribution and to better represent the *Dst* index variations [*Ebihara and Ejiri*, 2000] during the ring current buildup and decay.

[39] **Acknowledgments.** We would like to thank K. Ogilvie and R. Lepping for the use of Wind data in this paper, World Data Center C2 for Geomagnetism, Kyoto, for the provisional *AE* and *Dst* indices data, H. Singer for the GOES 8 and 9 magnetic field data, and C. Russell for the Polar magnetic field data. The data were obtained from the Coordinated Data Analysis Web (CDAWeb). This work was supported by the Academy of Finland. The work by N. Ganushkina was party supported by grant 00-15-96-623 from the Russian Foundation for Basic Researches, by INTAS grant 99–0078. Work at UCLA was supported by the National Aeronautics and Space Administration under research grant NAG5-7721.

[40] Michel Blanc thanks Takesi Iijima and Masaki Ejiri for their assistance in evaluating this paper.

References

Akasofu, S.-I., J. C. Cain, and S. Chapman, The magnetic field of a model radiation belt, numerically computed, *J. Geophys. Res.*, *66*, 4013–4026, 1961.

Alexeev, I. I., E. S. Belenkaya, V. V. Kalegaev, Y. I. Feldstein, and A. Grafe, Magnetic storms and magnetotail currents, *J. Geophys. Res.*, *101*, 7737–7747, 1996.

Antonova, A. Y., and V. P. Shabansky, Structure of the geomagnetic field at great distances from the Earth, *Geomagn. Aeron.*, *5*, 639–647, 1968.

Berko, F. W., L. J. Cahill Jr., and T. A. Fritz, Protons as the prime contributors to storm time ring current, *J. Geophys. Res.*, *80*, 3549–3552, 1975.

Crooker, N. U., and G. L. Siscoe, Birkeland currents as the cause of the low-latitude asymmetric disturbance field, *J. Geophys. Res.*, *86*, 11,201–11,210, 1981.

Ebihara, Y., and M. Ejiri, Simulation study on fundamental properties of the storm-time ring current, *J. Geophys. Res.*, *105*, 15,843–15,859, 2000.

Fairfield, D. H., M. H. Acuna, L. J. Zanetti, and T. A. Potemra, Magnetic field of equatorial midnight: AMPTE/CCE observations at $R < 8.8R_E$, *J. Geophys. Res.*, *92*, 7432–7442, 1987.

Ganushkina, N. Y., T. I. Pulkkinen, V. F. Bashkirov, D. N. Baker, and X. Li, Formation of intense nose structures, *Geophys. Res. Lett.*, *28*, 491–494, 2001.

Ganushkina, N. Y., T. I. Pulkkinen, and M. V. Kubyshkina, Storm time ring current magnetic field modeling during May 15, 1997 event, *Adv. Space Phys.*, in press, 2002.

Garcia, H. A., and W. N. Spjeldvik, Anisotropy characteristics of geomagnetically trapped ions, *J. Geophys. Res.*, *90*, 347–358, 1985.

Harel, M., R. A. Wolf, R. W. Spiro, P. H. Reiff, and C.-K. Chen, Quantitative simulation of a magnetospheric substorm, 2, Comparison with observations, *J. Geophys. Res.*, *86*, 2242–2260, 1981.

Hilmer, R. V., and G.-H. Voigt, A magnetospheric magnetic field model with flexible current systems driven by independent physical parameters, *J. Geophys. Res.*, *100*, 5613–5626, 1995.

Hoffman, R. A., and P. A. Bracken, Magnetic effects of the quiet-time proton belt, *J. Geophys. Res.*, *70*, 3541–3556, 1965.

Hoffman, R. A., and P. A. Bracken, Higher-order ring currents and particle energy storage in the magnetosphere, *J. Geophys. Res.*, *72*, 6039–6049, 1967.

Iijima, T., T. A. Potemra, and L. J. Zanetti, Large-scale characteristics of magnetospheric equatorial currents, *J. Geophys. Res.*, *95*, 991–999, 1990.

Jordanova, V. K., et al., October 1995 magnetic cloud and accompanying storm activity: Ring current evolution, *J. Geophys. Res.*, *103*, 79–92, 1998.

Kosik, J. C., Quantitative magnetic field models including magnetospheric ring current, *J. Geophys. Res.*, *94*, 12,021–12,026, 1989.

Langel, R. A., and R. E. Sweeney, Asymmetric ring current at twilight local time, *J. Geophys. Res.*, *76*, 4420–4427, 1971.

Lui, A. T. Y., R. W. McEntire, and S. M. Krimigis, Evolution of the ring current during two geomagnetic storms, *J. Geophys. Res.*, *92*, 7459–7470, 1987.

Mead, G., and D. H. Fairfield, A quantitative magnetospheric model derived from spacecraft magnetometer data, *J. Geophys. Res.*, *80*, 523–534, 1975.

Olson, W. P., and K. A. Pfitzer, A quantitative model of the magnetospheric magnetic field, *J. Geophys. Res.*, *79*, 3739–3748, 1974.

Parker, E. N., Newtonian development of the dynamical properties of the ionised gases at low density, *Phys. Rev.*, *107*, 924–933, 1957.

Pulkkinen, T. I., D. N. Baker, R. J. Pellinen, J. Buehner, H. E. J. Koskinen, R. E. Lopez, R. L. Dyson, and L. A. Frank, Particle scattering and current sheet stability in the geomagnetic tail during the substorm growth phase, *J. Geophys. Res.*, *97*, 19,283–19,297, 1992.

Roederer, J. G., *Dynamics of Geomagnetically Trapped Radiation*, 36 pp., Springer-Verlag, New York, 1970.

Roelof, E. C., Energetic neutral atom image of astorm-time ring current, *Geophys. Res. Lett.*, *14*, 652–655, 1987.

Speiser, T. W., and N. F. Ness, The neutral sheet in the geomagnetic tail: Its motion, equivalent currents, and field line connection through it, *J. Geophys. Res.*, *72*, 131–141, 1967.

Stern, D. P., Representation of magnetic fields in space, *Rev. Geophys.*, *14*, 199–214, 1976.

Sugiura, M., Equatorial current sheet in the magnetosphere, *J. Geophys. Res.*, *77*, 6093–6103, 1972.

Sugiura, M., and D. J. Poros, A magnetospheric field model incorporating the OGO 3 and 5 magnetic field observations, *Planet. Space Sci.*, *21*, 1763–1773, 1973.

Tsyganenko, N. A., Global quantitative models of the geomagnetic field in the cislunar magnetosphere for different disturbance levels, *Planet. Space Sci.*, *35*, 1347–1358, 1987.

Tsyganenko, N. A., A magnetospheric magnetic field model with a warped tail current sheet, *Planet. Space Sci.*, *37*, 5–20, 1989.

Tsyganenko, N. A., Quantitative models of the magnetospheric magnetic field: Methods and results, *Space Sci. Rev.*, *54*, 75–186, 1990.

Tsyganenko, N. A., Modeling the Earth's magnetospheric magnetic field confined within a realistic magnetopause, *J. Geophys. Res.*, *100*, 5599–5612, 1995.

Tsyganenko, N. A., and M. Peredo, Analytical models of the magnetic field of disk-shaped current sheets, *J. Geophys. Res.*, *99*, 199–205, 1994.

Tsyganenko, N. A., and A. V. Usmanov, Determination of the magnetospheric current system parameters and development of experimental geomagnetic field models based on data from IMP and HEOS satellites, *Planet. Space Sci.*, *30*, 985–998, 1982.

Tsyganenko, N. A., and A. V. Usmanov, Effects of the dayside field-aligned currents in location and structure of polar cusps, *Planet. Space Sci.*, *32*, 97–104, 1984.

Tsyganenko, N. A., G. Le, C. T. Russell, and T. Iyemori, A study of the inner magnetosphere based on data of Polar, *J. Geophys. Res.*, *104*, 10,275–10,283, 1999.

Voigt, G.-H., A mathematical magnetospheric field model with independent physical parameters, *Planet. Space Sci.*, *29*, 1–20, 1981.

N. Y. Ganushkina and T. I. Pulkkinen, Geophysical Research, Finnish Meteorological Institute, PO Box 503, Helsinki, FIN-00101, Finland. (Nataly.Ganushkina@fmi.fi; Tuija.Pulkkinen@fmi.fi)

M. V. Kubyshkina, Institute of Physics, University of St.-Petersburg, 198904 St.-Petersburg, Russia. (kubysh@snoopy.phys.spbu.ru)

C. T. Russell, Institute of Geophysics and Planetary Physics, University of California, Los Angeles, CA 90095-1567, USA. (ctrussell@igpp.ucla.edu)

H. J. Singer, NOAA Space Environment Center, Boulder, CO 80303-3328, USA. (Howard.Singer@noaa.gov)

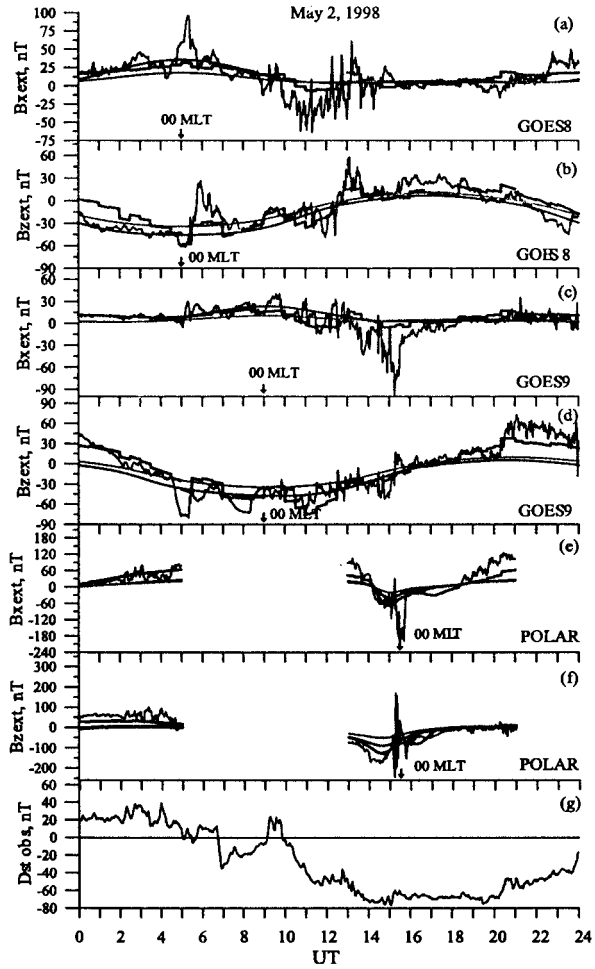

Figure 4. The B_x and B_z components of measured external magnetic field (solid black lines), modeled with bean-shaped ring current and variations of other current systems as described above (red lines) and modeled using Tsyganenko (T89) magnetic field model for Kp = 2 (green lines) and Kp = 4 (blue lines) for (a, b) GOES 8, (c, d) GOES 9, and (e, f) Polar measurements when data were available during storm event on May 2, 1998, with (g) the *Dst* index variations.

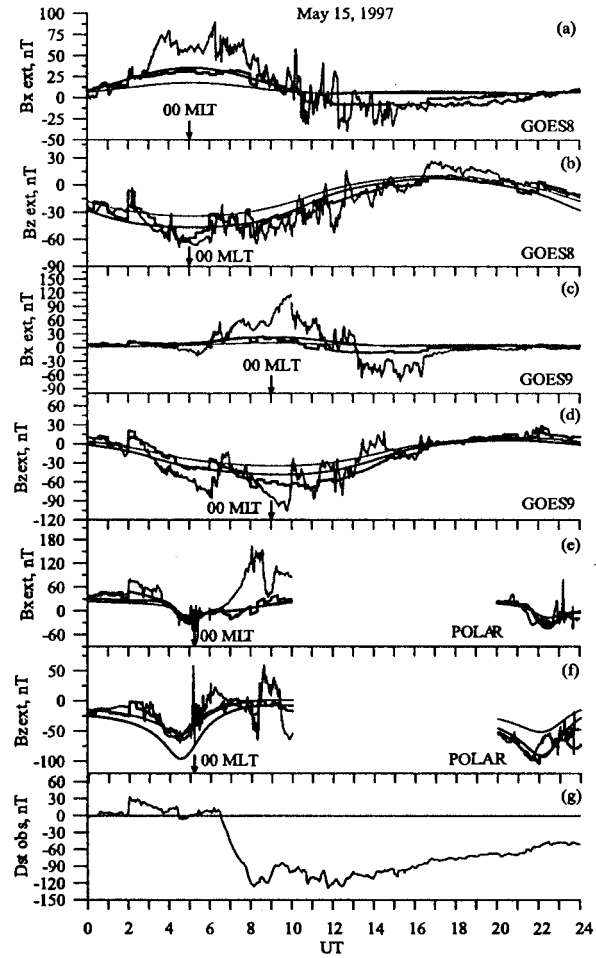

Figure 7. The B_x and B_z components of the measured external magnetic field (solid black lines), modeled with the bean-shaped ring current and variations of other current systems as described above (red lines) and modeled using Tsyganenko (T89) magnetic field model for Kp = 2 (green lines) and Kp = 4 (blue lines) for (a, b) GOES 8, (c, d) GOES 9, and (e, f) Polar measurements when data were available with (g) the *Dst* index variations during the modeled event on May 15, 1997.

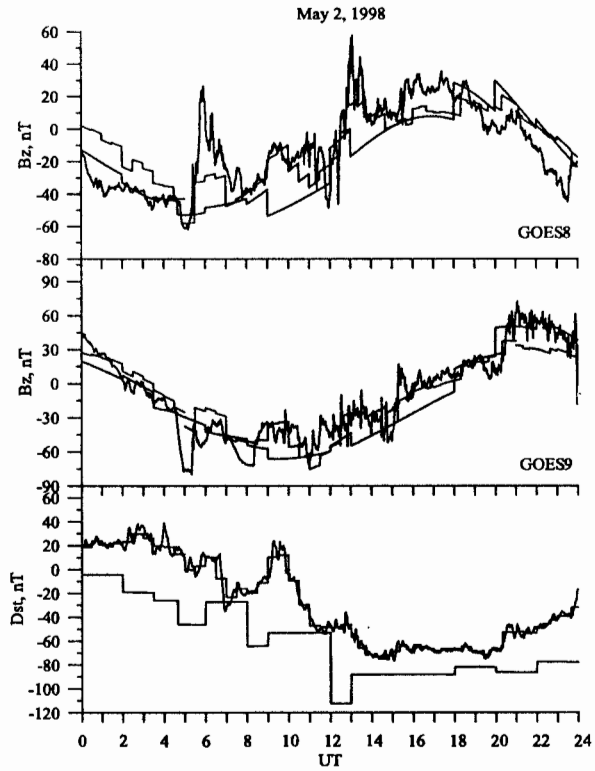

Figure 9. Observed B_z component of magnetic field (black lines), that modeled by using the bean-shaped ring current (red lines), and that calculated using the T96 model (pink lines) for GOES 8 data (top panel) and GOES 9 data (middle panel). The bottom panel shows the corresponding *Dst* index for the storm event on May 2, 1998.